CMIP6 Model-Based Assessment of Anthropogenic Influence on the Long Sustained Western Cape Drought over 2015–19

Jonghun Kam, Seung-Ki Min, Piotr Wolski, and Jong-Seong Kug

AFFILIATIONS: Kam, Min, and Kug—Division of Environmental Science and Engineering, Pohang University of Science and Technology, Pohang, South Korea; **Wolski**—Climate System Analysis Group, University of Cape Town, Cape Town, South Africa

CORRESPONDING AUTHOR: Jonghun Kam, jhkam@postech.ac.kr

DOI:10.1175/BAMS-D-20-0159.1

A supplement to this article is available online (10.1175/BAMS-D-20-0159.2)

CMIP6 simulations suggest that anthropogenic greenhouse gas forcing has at least doubled the likelihood of 2015–19 like prolonged droughts over the South African Western Cape, with large cancellation due to other anthropogenic effects.

South Africa's Western Cape (WC) with its agriculture-based economy and reservoir-based water supply system, is vulnerable to drought, and during 2015–19 it experienced a multiyear drought condition. A recent study (Otto et al. 2018) reported that anthropogenic influence increased the likelihood of exceeding rainfall reduction over the Cape Town region during the first three years of that drought (2015–17) by a factor of 3. During that period, Cape Town experienced a water crisis threatening

a shutdown of water supply to the four million residents (Masante et al. 2018) with water supply dropping to 20% of capacity in January 2018 (Muller 2018). In 2019, the WC experienced further dry conditions, extending the earlier drought and resulting in 2019 crop yield reduction by 25% (AGRI SA 2020).

The recent anthropogenic warming (IPCC 2018) likely caused drying trends over Southern Hemisphere subtropics associated with Hadley cell expansion (Purich et al. 2013; Burls et al. 2019) and is expected to increase drought durations over South Africa in the future (e.g., Ukkola et al. 2020). However, understanding of anthropogenic influence on the observed prolonged drought duration (e.g., multiple years) remains limited. Here, we investigate anthropogenic impact on meteorological drought *duration* in the broader WC region, posing the following questions: How unusual is the duration of the 2015–19 WC drought? Is there an anthropogenic contribution, particularly the contribution of greenhouse gas increases, to such prolonged droughts? By answering these questions, this study provides actionable information to policy makers and local stakeholders for drought mitigation and management.

Data and methods.

First, we computed regional averages of monthly precipitation over the WC from CRU (version TS v4.04; Harris et al. 2014), GPCC (version 2018; Schneider et al. 2011), and GPCP (version 2.3; Adler et al. 2018) datasets, rather than from station observations that cover only the western (wetter) part of the WC (1933–2017; Wolski et al. 2020). We found some stations excluded in the CRU and GPCC data since 2000 and 2010, respectively. The impact of changing numbers of stations is lower in GPCC than in CRU over the WC (Wolski et al. 2020); also, GPCC includes fewer observational stations before 1950 and after 1998 than CRU (Otto et al. 2018). Nevertheless, an overall consistency is found between gridded data and station observations (Figs. 1a–c).

Next, we computed the 12-month Standard Precipitation Index (SPI-12) over the study region (Fig. 1f; McKee et al. 1993) as the WC drought index. SPI-12 threshold values of −0.8 and 0.2 were used to identify drought onset and recovery, respectively, following Mo (2011). We also computed the Standardized Precipitation Evapotranspiration Index (SPEI) using the CRU data and found no significant difference from SPI (not shown), confirming the dominant role of precipitation in determining the WC drought (Otto et al. 2018).

To identify anthropogenic influence on the long-lasting drought, five CMIP6 model simulations were analyzed over 1901–2019: historical (ALL; 32 ensemble runs), natural-only (NAT; 30), and greenhouse gas-only (GHG; 25), which give 289, 324, and 233 drought events, respectively. First, seven CMIP6 models were selected based on the availability of multiple ensemble members (≥3 members for ALL, NAT, and GHG; see Table ES1 in the online supplemental information) and then the five models were finally selected based on the performance of the seasonality of precipitation over WC (Fig. ES1). The ALL simulations (ended in 2014) were extended up to 2019 using the corresponding Shared Socioeconomic Pathway 2.45 or 3.70 scenario runs, which were chosen based on the data availability considering their similar radiative forcing over 2015–19 (O'Neill et al. 2016). The ALL simulations include anthropogenic (increases in greenhouse gases and aerosols) and natural forcings (changes in solar and volcanic activities) while the NAT simulations contain only natural forcings. The GHG simulations are driven by only greenhouse gas increases, designed to isolate responses to GHG forcing from other forcings including aerosols, solar, and volcanic forcings (Meinshausen et al. 2017).

We used an areal conservative remapping method to interpolate all model data onto the observed grids (50 km × 50 km) before taking WC area means, which accounts for fractional contributions of the input grid boxes to each output grid box. Next, we fitted gamma distribution to regional mean precipitation from ALL simulations and then used it to compute SPI-12 for the ALL, GHG, and NAT simulations of the corresponding

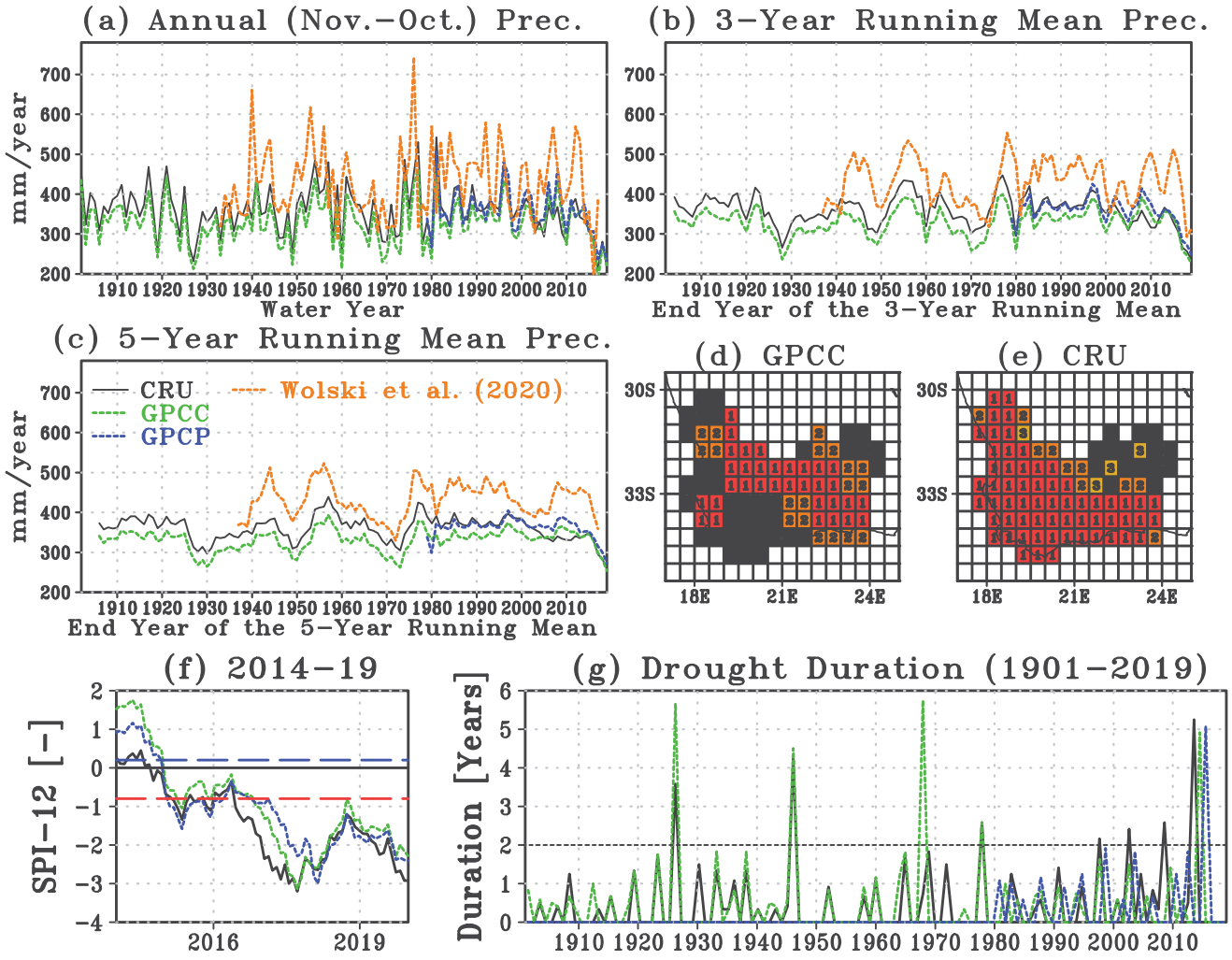

Fig. 1. Time series of the water year (WY; November through October of the following year) (a) total precipitation and the (b) 3-yr and (c) 5-yr running means of the WY annual total precipitation. In (a)–(c), orange dotted lines depict the stations data (1933–2017) used in Wolski et al. (2020). Also shown are ranks of the 5-yr mean precipitation over November 2014 through October 2019 from the (d) GPCC and (e) CRU data. Colored grid cells in (d) and (e) depict our study region, the Western Cape (red, orange, and yellow depict the lowest, second lowest, and third lowest, respectively, since 1901). Time series of monthly drought (SPI-12) index over 2014–19 (f). Red and blue dashed lines depict the threshold values for drought onset and recovery, respectively. (g) Duration of the observed drought events identified from the SPI-12 values: CRU (black), GPCC (green), and GPCP (blue).

model. Finally, we computed the duration of each drought event as done in the observations and compared the simulated frequency of long-term (≥2 yr) droughts [the ratio of the number of long-term drought events to the number of all drought events] within a 20-yr moving window (McCabe et al. 2004) with the observed.

To construct a multimodel probability distribution of drought duration, we used the last 30-yr segment (1990–2019) from the ALL, GHG, and NAT simulations and fitted the gamma distribution function to durations of identified drought events. We used the maximum likelihood estimation method for parameter estimation. Fitted gamma distributions are well matched with histograms of drought durations (positively skewed with a large range from months to years; see Fig. ES2).

We estimated the probability ratio of long-term drought duration [PR = (P_{ALL} or P_{GHG})/(P_{NAT}), where P_{ALL}, P_{GHG}, and P_{NAT} are the probabilities of exceeding the drought duration thresholds (2, 3, 4, or 5 years) from the ALL, GHG, and NAT ensemble runs, respectively]. We computed 90% confidence interval (CI) of PR using a bootstrap method.

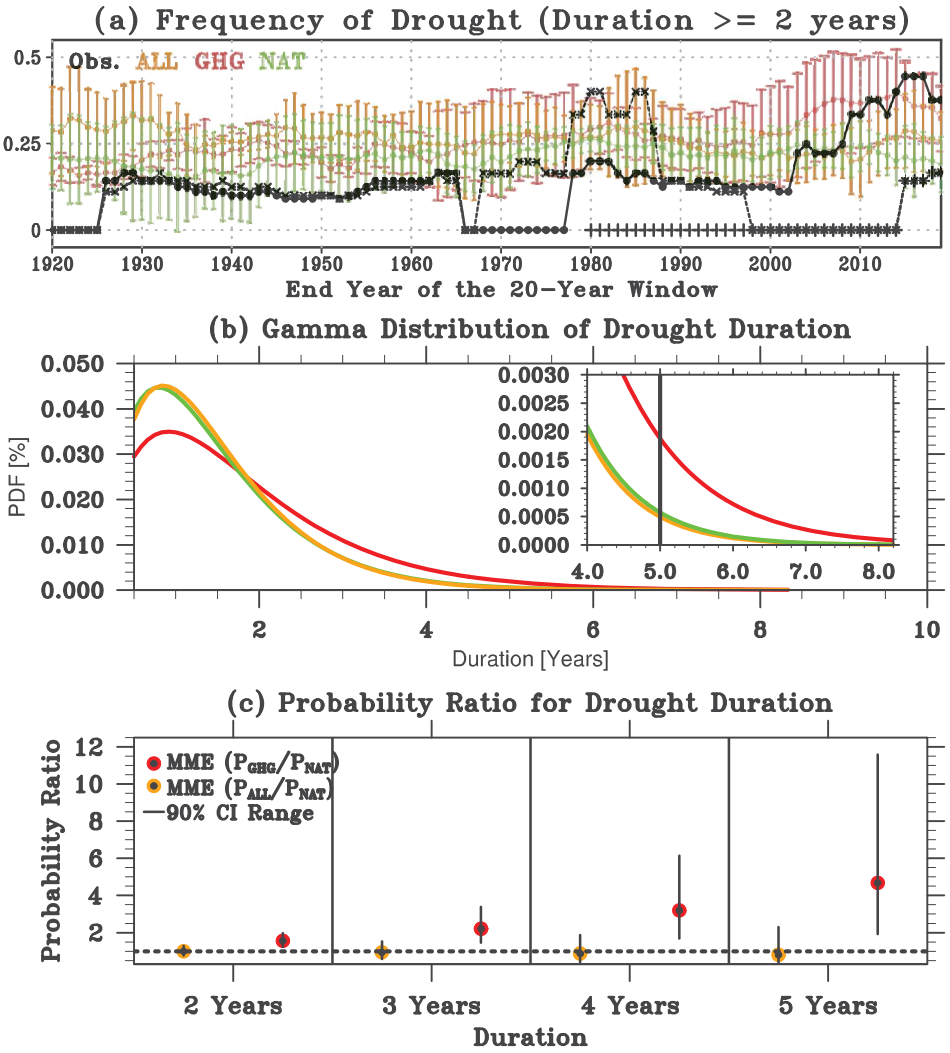

Fig. 2. (a) 20-yr moving averages of the frequency of long-term drought events from the observations (black circles, plus signs, and cross signs depicts CRU, GPCC, and GPCP, respectively) and the frequency of long-term drought events (divided by total number of drought events within the 20-yr moving window) from model simulations. Orange, red and green dots depict the MME drought frequency from the ALL, GHG, and NAT forcing runs, respectively. The error bars depict the range within plus or minus one standard deviation of the MME from each experiment runs. (b) Gamma distributions fitted to drought duration from the ALL (orange), GHG (red), and NAT (green) forcing runs over the 1990–2019 period (see Fig. ES2 for histograms). (c) Probability ratios (PRs) between ALL and NAT (orange) and between GHG and NAT (red) for drought duration ≥ 2, 3, 4, and 5 years, respectively. Lines indicate 90% confidence interval (CI) range of PRs. See text for details.

We first randomly select a sample (with repetition) of 289, 324, and 233 drought events from the fitted distribution of ALL, NAT, and GHG simulations, respectively. Then, we fit the gamma distribution to the drought durations of random samples and calculate P_{ALL}, P_{GHG}, and P_{NAT} and PRs. Finally, we repeated the entire procedure 10,000 times and estimated the 90% CI of PR.

Results.

The WC had anomalously low precipitation during the water year 2019 (WY 2019; defined based on precipitation's seasonality as November 2018–October 2019; Fig. 1a). WY 2019 is the second and fourth driest since 1901 in CRU and GPCC, respectively. Three- and five-year averages ending in 2019 are the driest in all three datasets

(Figs. 1b,c). The extremely long-lasting drought started in early 2015 and continued by WY 2017 (Otto et al. 2018). Rainfall in WY 2018 was still low but slightly higher than rainfall in WY 2016. The dry conditions during 2019 ranked the 2015–19 precipitation the lowest (since 1901) over 37% (GPCC) or 68% (CRU) area of WC (Figs. 1d,e), extending the 2015–17 drought to December 2019 (Fig. 1f).

We detected 41, 43, and 15 events over 119, 119, and 41 years from the CRU, GPCC, and GPCP precipitation-based drought index, respectively (Fig. 1g). The expected return period of identified droughts ranges from 2.7 (119 years/43 events or 41/15) to 2.9 years (119/41). CRU and GPCC share longest droughts over 1925–28, 1944–48, and 2015–19 but with different ranks. The 2015–19 drought duration is the longest (CRU) or third longest (GPCC) longest since 1901, with small differences (<4 months) among the observational data (63, 59, and 61 months from CRU, GPCC, and GPCP, respectively). GPCC and GPCP show no significant trend in the short-term (herein, <2 yr) and long-term (≥2 yr) drought frequencies. CRU shows that four out of seven long-term droughts occurred after 1995, but this might be partly due to station base changes identified by Wolski et al. (2020). The disparity between datasets warrants further investigation of uncertainty sources in gridded data.

The frequencies of long-term droughts in the GHG simulations show an upward trend since 2000 (consistent with the CRU data) while the ALL and NAT simulations show no trend over time (Fig. 2a). Over 1970s–1990s, high frequencies of long-term droughts in GPCC are consistent with those in the ALL and GHG simulations. The multimodel estimated gamma distribution (a red line in Fig. 2b) for GHG has a longer tail than that for the ALL or NAT simulations, with little difference found between ALL and NAT. This implies that the likelihood to have long sustained drought is significantly increased by GHG increases while other external forcing such as anthropogenic aerosols may offset the GHG-induced increase in long-term drought frequency.

The PR value from ALL and NAT simulations for 5-yr duration or longer is 0.8 (90% CI of 0.3–2.3; Fig. 2c). The PR estimates for the duration of two, three, and four years or longer are similar: 0.99 (0.8–1.3), 0.94 (0.6–1.6), and 0.9 (0.4–1.9), respectively. Little difference in PR between ALL and NAT suggests a lack of significant anthropogenic influence on multiyear drought frequencies over the WC region. In contrast, the PR estimates from GHG and NAT simulations show that greenhouse gas–induced warming increases the likelihood of droughts >5 years in duration (like the 2015–19 drought) by a factor of 4.7 (the 90% CI of 1.9 to 11.6). The PR estimates for the drought with duration of 2, 3, and 4 years or longer are also larger than unity: 1.6 (1.2–2.0), 2.2 (1.4–3.4), and 3.2 (1.7–6.1), respectively, supporting the important role of GHG forcing in driving long-lasting droughts.

In summary, the 2015–19 WC drought is the longest (either the longest or third longest) drought on record since 1901, and still continues as of the end of 2019. Based on the five CMIP6 simulations, which can reproduce the observed precipitation seasonality, GHG forcing has likely contributed to the increased probability of such long-lasting drought, at least by a factor of 2, compared to conditions without human influences (NAT). Results remain unaffected when including the two models that have lower performance in precipitation seasonality, suggesting weak sensitivity of our attribution results to model skills. Although some previous studies suggested Hadley cell expansion as a possible mechanism for increased duration of short-term droughts (Ukkola et al. 2020), historical simulations (ALL), including non-GHG anthropogenic forcings, do not show clear increases in the frequency of long-term droughts. It suggests possible offsetting effects by anthropogenic aerosols (cf. Rowell et al. 2015). Quantifying the relative contribution of GHG and other anthropogenic effects and exploring the associated physical mechanisms including Hadley expansion influence (Garfinkel et al. 2015; Nguyen et al. 2015; Zhao et al. 2020) as well as El Niño (Yuan et al. 2013; Otto et al. 2018) is an important task for the future risk assessment of the WC droughts.

Acknowledgments. We thank the CMIP6 project, for making available the CMIP6 data; and the Climate Research Unit and NOAA ESRL Physical Sciences Laboratory for providing observational precipitation datasets. J.K. and P.W. are partially supported by the NRF Basic Research Program (NRF-2020R1A4A1018818) and AXA Chair in African Climate Risk, respectively.

References

Adler, R. F., and Coauthors, 2018: The Global Precipitation Climatology Project (GPCP) monthly analysis (new version 2.3) and a review of 2017 global precipitation. *Atmosphere*, **9**, 138, https://doi.org/10.3390/atmos9040138.

AGRI SA, 2020: Agriculture Drought Report 2019/2020: "We are in a financial drought!" AGRI SA, 42 pp., https://rpo.co.za/wp-content/uploads/2019/12/Agriculture-Drought-Report-2019.pdf.

Burls, N. J., R. C. Blamey, B. A. Cash, E. T. Swenson, A. al Fahad, M. J. M. Bopape, D. M. Straus, and C. J. Reason, 2019: The Cape Town "Day Zero" drought and Hadley cell expansion. *npj Climate Atmos. Sci.*, **2**, 27, https://doi.org/10.1038/s41612-019-0084-6.

Eyring, V., S. Bony, Meehl, Senior, B. Stevens, Stouffer, and Taylor, 2016: Overview of the Coupled Model Intercomparison Project phase 6 (CMIP6) experimental design and organization. *Geosci. Model Dev.*, **9**, 1937–1958, https://doi.org/10.5194/gmd-9-1937-2016.

Garfinkel, C. I., D. W. Waugh, and L. M. Polvani, 2015: Recent Hadley cell expansion: The role of internal atmospheric variability in reconciling modeled and observed trends. *Geophys. Res. Lett.*, **42**, 10824–10831, https://doi.org/10.1002/2015GL066942.

Harris, I. P. D. J., P. D. Jones, T. J. Osborn, and D. H. Lister, 2014: Updated high-resolution grids of monthly climatic observations—The CRU TS3.10 dataset. *Int. J. Climatol.*, **34**, 623–642, https://doi.org/10.1002/joc.3711.

IPCC, 2018: Summary for policymakers. Global Warming of 1.5°C, V. Masson-Delmotte et al., Eds., World Meteorological Organization, 1–32.

Masante, D., N. McCormick, J. Vogt, C. Carmona-Moreno, E. Cordano, and I. Ameztoy, 2018: Drought and Water Crisis in Southern Africa. European Commission, Ispra, 28 pp., https://doi.org/10.2760/81873.

McCabe, G. J., M. A. Palecki, and J. L. Betancourt, 2004: Pacific and Atlantic Ocean influences on multidecadal drought frequency in the United States. *Proc. Natl. Acad. Sci. USA*, **101**, 4136–4141, https://doi.org/10.1073/pnas.0306738101.

McKee, T. B., N. J. Doesken, and J. Kleist, 1993: The relationship of drought frequency and duration to time scales. Proc. Eighth Conf. on Applied Climatology, Anaheim, CA, Amer. Meteor. Soc., 179–184.

Meinshausen, M., and Coauthors, 2017: Historical greenhouse gas concentrations for climate modelling (CMIP6). *Geosci. Model Dev.*, **10**, 2057–2116, https://doi.org/10.5194/gmd-10-2057-2017.

Mo, K. C., 2011: Drought onset and recovery over the United States. *J. Geophys. Res.*, **116**, D20106, https://doi.org/10.1029/2011JD016168.

Muller, M., 2020: Cape Town's drought: Don't blame climate change. *Nature*, **559**, 174–176, https://doi.org/10.1038/d41586-018-05649-1.

Nguyen, H., C. Lucas, A. Evans, B. Timbal, and L. Hanson, 2015: Expansion of the Southern Hemisphere Hadley cell in response to greenhouse gas forcing. *J. Climate*, **28**, 8067–8077, https://doi.org/10.1175/JCLI-D-15-0139.1.

O'Neill, B. C., and Coauthors, 2016: The Scenario Model Intercomparison Project (ScenarioMIP) for CMIP6. *Geosci. Model Dev.*, **9**, 3461–3482, https://doi.org/10.5194/gmd-9-3461-2016.

Otto, F. E., and Coauthors, 2018: Anthropogenic influence on the drivers of the Western Cape drought 2015–2017. *Environ. Res. Lett.*, **13**, 124010, https://doi.org/10.1088/1748-9326/aae9f9.

Purich, A., T. Cowan, S. Min, and W. Cai, 2013: Autumn precipitation trends over Southern Hemisphere midlatitudes as simulated by CMIP5 models. *J. Climate*, **26**, 8341–8356, https://doi.org/10.1175/JCLI-D-13-00007.1.

Rowell, D. P., B. B. B. Booth, S. E. Nicholson, and P. Good, 2015: Reconciling past and future rainfall trends over East Africa. *J. Climate*, **28**, 9768–9788, https://doi.org/10.1175/JCLI-D-15-0140.1.

Schneider, U., A. Becker, P. Finger, A. Meyer-Christoffer, B. Rudolf, and M. Ziese, 2011: GPCC full data reanalysis version 6.0 at 0.5: Monthly land-surface precipitation from rain-gauges built on GTS-based and historic data. GPCC, accessed 6 October 2020, https://doi.org/10.5676/DWD_GPCC/FD_M_V6_050.

Stott, P. A., D. A. Stone, and M. R. Allen, 2004: Human contribution to the European heatwave of 2003. *Nature*, **432**, 610–614, https://doi.org/10.1038/nature03089.

Ukkola, A. M., M. G. De Kauwe, M. L. Roderick, G. Abramowitz, and A. J. Pitman, 2020: Robust future changes in meteorological drought in CMIP6 projections despite uncertainty in precipitation. *Geophys. Res. Lett.*, **47**, e2020GL087820, https://doi.org/10.1029/2020GL087820.

Wolski, P., S. Conradie, C. Jack, and M. Tadross, 2020: Spatio-temporal patterns of rainfall trends and the 2015–2017 drought over the winter rainfall region of South Africa. *Int. J. Climatol.*, https://doi.org/10.1002/joc.6768, in press.

Yuan, X., E. F. Wood, N. W. Chaney, J. Sheffield, J. Kam, M. Liang, and K. Guan, 2013: Probabilistic seasonal forecasting of African drought by dynamical models. *J. Hydrometeor.*, **14**, 1706–1720, https://doi.org/10.1175/JHM-D-13-054.1.

Zhao, X., Allen, T. Wood, and Maycock, 2020: Tropical belt width proportionately more sensitive to aerosols than greenhouse gases. *Geophys. Res. Lett.*, **47**, e2019GL086425, https://doi.org/10.1029/2019GL086425.